LA-UR-20-24244
Approved for public release; distribution is unlimited.

Title: Irradiation enhanced diffusion and diffusional creep in U3Si2

Author(s): Cooper, Michael William Donald
Gamble, K A
Matthews, Christopher
Andersson, Anders David Ragnar

Intended for: Report

Issued: 2020-06-11

Irradiation enhanced diffusion and diffusional creep in U_3Si_2

M. W. D. Cooper[a], K. A. Gamble[b], C. Matthews[a], and D. A. Andersson[a]

[a]*Materials Science and Technology Division, Los Alamos National Laboratory*
[b]*Fuel Modeling and Simulation, Idaho National Laboratory*

June 1, 2020

Executive Summary

U_3Si_2 is a candidate as an advanced fuel for light water reactors (LWRs). Compared to UO_2, there are significant data gaps for the thermophysical and thermomechanical properties of U_3Si_2. Atomic scale simulations can help fill in those gaps, while also providing a more mechanistic understanding of the material properties. Creep is an important property for fuel performance as it influences the pellet-cladding gap, which in turn affects the temperature of the fuel (a key parameter in many other aspects of fuel behavior). In this work, we employed a DFT-informed cluster dynamics framework to predict point defect concentrations in U_3Si_2. The concentrations, diffusivities, and volumes of these defects were used to develop a diffusional creep model based on bulk (Nabarro-Herring) and grain boundary (Coble) diffusion processes. It was found that irradiation enhanced Nabarro-Herring creep is dominant at low temperatures, while Coble creep dominates for high temperatures. The model compares well against available experimental data and has been implemented in BISON. A demonstration case using simple power profiles has been carried out, showing that negligible creep occurs due to the low temperatures experienced by U_3Si_2, a consequence of its high thermal conductivity.

Contents

List of Figures

1 Introduction

Nuclear fuel must operate within well-defined criteria under the extreme conditions created within a reactor. During the lifetime of nuclear fuel it undergoes significant compositional change, high levels of radiation damage, and experiences extreme heat flux (due to fission and decay heat). The latter, in combination with the poor thermal conductivity of UO_2 (especially at high burnup), creates extreme temperature gradients. As such, despite the high melting point of UO_2 the possibility of centerline melting is a concern during accident conditions. Fuels that exhibit higher thermal conductivity benefit from a reduced risk of fuel melting. Typically materials without a bandgap, such as uranium intermetallics, are suitable due to high electronic heat transfer that, compared to phonon transport, is not as strongly affected by defects in the lattice.

Uranium silicide compounds have been widely used in low temperature research reactors, typically as dispersion fuels within an aluminum matrix [5–10]. U_3Si_2 has replaced the more uranium dense U_3Si due to its reduced in-pile swelling [11–18]. More recently, U_3Si_2 has been considered as an accident tolerant fuel candidate for light water reactors (LWRs) due to its high thermal conductivity [4] and high uranium denisty. While these properties highlight the potential benefits of U_3Si_2 as an LWR fuel concept, work must be done to address the reaction of U_3Si_2 with steam [19, 20]. Another important factor for fuel safety is the creep of the pellet, which impacts the stress imparted on the clad by the pellet. Therefore, understanding the underlying processes to quantify creep in advanced fuels, such as U_3Si_2, is critical to understanding the extent of their accident tolerance.

Diffusional creep has two contributions: i) bulk diffusion (Nabarro-Herring creep [21]) and ii) grain boundary diffusion (Coble creep [22]). Both of these processes are driven by the response of defect diffusion to an applied stress. Vacancies (interstitials) migrate away from (towards) tensile regions and towards (away from) compressive regions. This results in net self-diffusion from the compressive region to the tensile region, leading to diffusional creep. U_3Si_2 creep models have previously been derived from experimental data [2,3]. The framework used by Metzger [3] can take diffusivity data from either experiment or modeling. By developing an understanding of defect concentrations and their mobility in the bulk lattice or in the grain boundaries, both Nabarro-Herring and Coble creep can be examined using atomic scale techniques.

Atomic scale simulations have proved effective at giving insight into the atomic scale processes that govern dffusion in UO_2 fuel. Density functional theory (DFT) calculations give a good comparison to experiment for D_1 [23–25]. By using the DFT data from Perriot et al. [25] to parameterize a Free Energy Cluster Dynamics (FECD) framework, Matthews et al. [26, 27] were able to simulate the D_2 diffusion regime for the first time, showing that large Xe bearing clusters stabilized under irradiation were critical. The same approach has also been applied to U self-diffusion in UO_2 [26] and helped inform understanding of Nabarro-Herring creep in doped UO_2 [28]. Classical MD simulations of electron and ballistic stopping have been employed to study the athermal D_3 diffusion regime of self and Xe diffusion [29–31].

To support the development of accident tolerant fuel performance codes, the same mix of atomic scale simulation techniques can be applied to predict defect and diffusion behavior in U_3Si_2. Andersson et al. [32] have used DFT to show that Xe is highly insoluble in U_3Si_2 and predict D_1 for U, Si and Xe. They found that for a given temperature intrinsic Xe diffusion, D_1, is greater for U_3Si_2 than UO_2. By studying D_1, Andersson et al. [32] generated all the defect energy data necessary to parameterize the cluster dynamics framework of Matthews et al. [26,27] for the study of D_2 diffusion in U_3Si_2, as was demonstrated in a recent milestone [33].

In this work, the cluster dynamics simulations for U_3Si_2 have been updated and used to predict point defect concentrations and diffusivities for in-reactor conditions. The defect diffusivities prediced by Andersson et al. [32] and the enhanced defect concentrations predicted here were combined within a framework similar to that of Metzger [3] to develop a multiscale model for diffusional creep of U_3Si_2. The model was validated against available experimental data and has been implemented in BISON to demonstrate its application for $U3Si_2$ fuel performance using a simple power profile.

2 Method

2.1 Cluster dynamics framework

Cluster dynamics simualtions were carried out using the Free Energy Cluster Dynamics (FECD) framework developed by Matthews et al. [26, 27] and implemented in the Centipede code. The framework has been applied to the simulation of defect concentrations and diffusivities contributing to self-diffusion [26] and Xe diffusion [27] in UO_2 under irradiation. Their results demonstrate the successful application of this framework to capture the D_1-D_2 transition for self- and Xe diffusion. A detailed description of the framework can be found elsewhere [26,27], however a brief description of the method and its application to U_3Si_2 will be given here.

The concentrations of defects in the system are considered by solving a set of ordinary differential equations (ODEs) that capture a number of phenomena including: production of Frenkel pairs through irradiation, mutual recombination of Frenkel pairs, interaction with sinks, and clustering of point defects. For given defect, x_d, the ODE can be expressed as:

$$\frac{dx_d}{dt} = \dot{\beta}_d + \sum_C \dot{R}_{d,C}(x_d, x_C, T, G) - \sum_s \dot{S}_{d,s}(x_d, x_s, T, G) \tag{2.1}$$

where $\dot{\beta}_d$ describes the source rate of defects through irradiation. $\dot{R}_{d,C}$ and $\dot{S}_{d,s}$ are the cluster and sink rates, which are summed across individual cluster and sink types, respectively. The Centipede code finds the steady-state solution to this coupled set of ODEs, such that $\frac{dx_d}{dt} \leq A$ for all defects, where A is a convergence criteria. An individual reaction, $\dot{R}_d$, can be expressed as:

$$\dot{R}_d = \begin{cases} \frac{k_i^2}{\Omega} D x_A x_B \left[1 - exp\left(\frac{f}{k_B T}\right)\right], & \text{if } f < 0, \\ \frac{k_i^2}{\Omega} D x_Y x_Z \left[exp\left(\frac{f}{k_B T}\right) - 1\right], & \text{otherwise} \end{cases} \tag{2.2}$$

where Ω is the atomic volume, k_i is a reaction rate constant, $D = D_A + D_B$ is the sum of the diffusivities of the reactants, x_A and x_B are the atom fractions of the reactants and x_Y and x_Z are the atom fractions of the products. If $f < 0$ the net rate is for the reaction to go forwards and otherwise it goes backwards. The driving force is given by the change in the free energy of the system due to the reaction:

$$f = \sum_{p=1}^{P} \frac{\partial G}{\partial x_p} - \sum_{r=1}^{R} \frac{\partial G}{\partial x_r} \tag{2.3}$$

where P and R are the set of products, p, and reactants, r, respectively. A detailed explanation of Eqs. (2.1) to (2.3) and their application to Xe in UO_2 is given in Refs. [26, 27].

In this work, the FECD framework is applied it to the simulation of irradiation enhanced defect concentrations and diffusion in U_3Si_2. One of the key differences with the original application to UO_2 is that, due to the relatively low mobility of U and Si vacancies, the defect concentrations on both the U and Si sublattices must be tracked. Conversely, in the UO_2 system both interstitials and vacancies on the oxygen sublattice migrate so quickly that interaction with sinks and mutual recombination maintains thermal equilibrium concentrations. Given that two sublattices are tracked there are now three dependent variables that represent the perfect lattice sites: U_U, Si_{Si}, and V_i. Antisite defects are omitted to limit the number of solved variables and ODEs. The defects and reactions solved for in FECD are as follows:

Solved point defects variables: U_i, V_U, Si_i, V_{Si}

Dependent variables: U_U, Si_{Si}, V_i

Reactions of U and Si defect with sinks:

$$sink + U_i \leftrightarrow sink + V_i \tag{2.4}$$

$$sink + Si_i \leftrightarrow sink + V_i \tag{2.5}$$

$$sink + V_U \leftrightarrow sink + U_U \tag{2.6}$$

$$sink + V_{Si} \leftrightarrow sink + Si_{Si} \tag{2.7}$$

Annihilation of interstitials and vacancies:

$$U_i + V_U \leftrightarrow U_U + V_i \tag{2.8}$$

$$Si_i + V_{Si} \leftrightarrow Si_{Si} + V_i \tag{2.9}$$

The sink and source strengths are unchanged from the application to UO_2 in an LWR.

2.2 U and Si defect parameters

Cluster dynamics simulations were carried out to investigate the diffusivity of individual defects that may contribute to diffusional creep: U_i, Si_i, V_U, and V_{Si}. The defect stability and mobility influence the behavior of the defects during the cluster dynamics simulation. The thermodynamic stability of the defects is given by the formation enthalpy and entropy taken from Ref. [32], and are summarized in Table 2.1. The U_3Si_2 system contains two symmetrically unique uranium lattice sites. To simplify the cluster dynamics simulation, only the most stable V_U site (2a) was considered for the total V_U concentration. Previously, the concentrations had been treated as per site values [32]. However, for the purposes of the cluster dynamics simulations it is important to account for the fact that there are not the same number of sites available to each defect in a given volume. Therefore, the concentration of the defect is adjusted to account for the number of sites per formula unit, n. Under thermal equilibrium in the dilute limit, the defect concentration, $[x]$, of defect x is given by the Arrhenius function:

$$[x] = n \cdot \exp\left(\frac{-H_f + S_f T}{k_B T}\right) \tag{2.10}$$

where H_f is the enthalpy of formation, S_f is the entropy of formation, k_B is the Boltzmann constant, and T is the temperature.

Table 2.1: Point defect formation energies and entropies used in the cluster dynamics model.

Defect	H_f (eV)	S_f (k_B)	n
U_i	0.87	-3.15	2
V_U	1.69	0.45	1
Si_i	0.55	2.19	1
V_{Si}	1.79	6.28	2

Table 2.2: Parameters that describe the defect diffusivities used in the cluster dynamics model.

Defect	H_{mig} (eV)	v_{mig} (Hz)	α (Å)	ξ	Z
U_i	0.31	1.51×10^{14}	3.80	2	4
V_U	1.21	1.40×10^{13}	3.90	1	2
Si_i	1.80	1.00×10^{13}	5.18	2	4
V_{Si}	2.37	1.00×10^{13}	4.19	2	4

In addition to the thermal stability defined by H_f, S_f, and n, the diffusivity of individual defects, D_x, must be known in order to determined the irradiation enhanced defect concentrations. This is defined by the defect migration barrier (H_{mig}), attempt frequency (v_{mig}), number of jump directions (Z), the jump distance (α), and the dimensionality of diffusion (ξ), as such:

$$D_x = \frac{Z}{2\xi}\alpha^2 v_{mig} \exp\left(\frac{-H_{mig}}{k_B T}\right) \tag{2.11}$$

In U_3Si_2 there are two unique crystallographic directions for diffusion. For defining the rates within the cluster dynamics framework the fastest of the two directions for each defect was taken and the relevant parameters are summarized in Table 2.2.

2.3 BISON simulations

Here, a small 10-pellet fuel rodlet was analyzed. The cladding is taken as Zircaloy-4. The rodlet was modeled using a 2D-RZ axisymmetric representation of the fuel and cladding. Tabel 2.3 lists the geometry of the rodlet, initial conditions of the fill gas, and the operational conditions of the coolant (representative of a PWR). The initial value of grain-size for the U_3Si_2 fueled rodlet was chosen based upon the observations from Shimizu's data upon which the coupled swelling model was developed [34]. The power supplied to the fuel was linearly increased from zero to its maximum value over 10000 seconds for the fresh fuel cases. It was then held at the maximum values for 3.2 years. The multiscale creep model developed in the report was used.

Table 2.3: Rodlet specifications for normal operation simulations in BISON.

	Value	Units
Number of pellets	10	-
Fuel enrichment	5	%
Pellet length	9.83	mm
Pellet outer diameter	8.19	mm
Radial gap width	82.55	μm
Clad thickness	0.572	mm
Rodlet diameter	9.5	mm
Initial fill pressure	2	MPa
Initial fill gas	Helium	-
Plenum height	26	mm
Initial fuel grain radius	25	μm
Coolant inlet mass flux	3800	kg/m^2-s
Coolant inlet temperature	580	K
Coolant pressure	15.5	MPa

3 Results and Discussion

3.1 Cluster dynamics simulations

The concentrations of V_U, U_i, V_{Si}, and Si_i under irradiation conditions typical of a LWR have been assessed using cluster dynamics and are shown in Fig. 3.1. The results will not be discussed in detail as similar results have been covered in a previous milestone [33]. However, given some of the parameters in the cluster dynamics model have been updated since then, a brief overview of the new results will be given here. Fig. 3.1 shows that at high temperatures all defects are at their thermal equilibrium concentrations. As the temperature decreases, irradiation enhancement of first V_{Si}, then V_U, and then Si_i, occurs. These enhanced concentrations will influence the low temperature diffusional creep rate, as studied in Section 3.2.

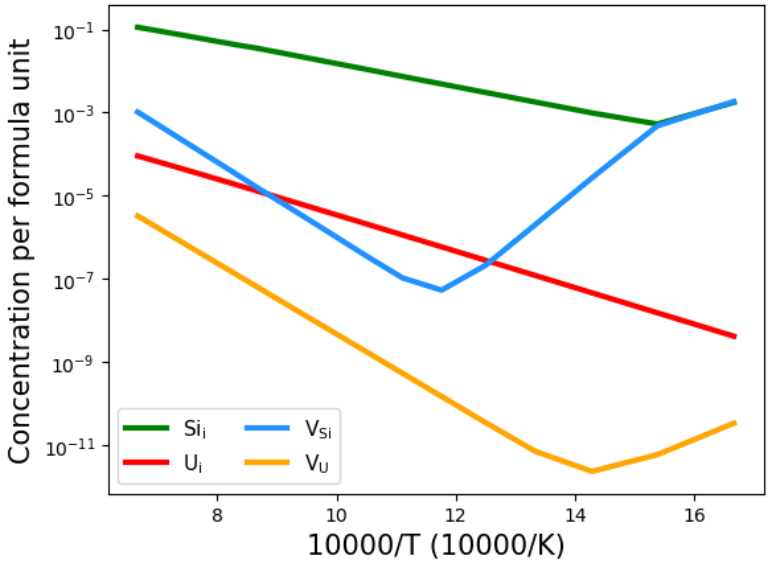

Figure 3.1: The irradiation enhanced point defect concentrations in U_3Si_2 from cluster dynamics simulations.

By multiplying the defect concentrations shown in Fig. 3.1 with the diffusivities of the defects in the fastest crystallographic direction (given by Eq. (2.11) and the parameters in Table 2.2), the self-diffusivities are determined, as shown in Fig. 3.2. It can be seen that the self-diffusivity due to interstitials is much greater than that due to vacancies. Additionally, the irradiation enhanced regime is broadly athermal, as discussed in the previous milestone [33]. These results represent the contributions of the defects to self-diffusion and, as discussed later, is different to the diffusivities used for creep (where the rate limiting crystallographic direction is dominant).

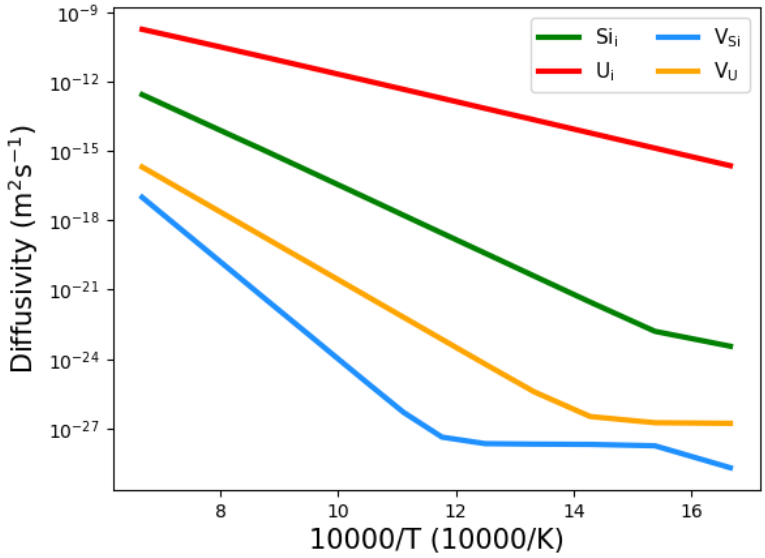

Figure 3.2: The irradiation enhanced self-diffusivity due to point defects in U_3Si_2 from cluster dynamics simulations.

3.2 Diffusional creep model

The defect concentrations calculated from the cluster dynamics simulations can be analyzed to understand thermal and irradiation enhanced contributions to bulk diffusional creep (Nabarro-Herring creep). Nabarro-Herring creep is due to the diffusion of point defects under an elastic strain. The direction of the diffusion of a point defect is determined by the sign of the defect volume (change in lattice volume upon formation of the defect). Defects that contract (expand) the lattice are more favorably in regions of compressive (tensile) strain. Given that in U_3Si_2 vacancies (interstitials) contract (expand) the lattice, the flow of mass is from the compressive to the tensile region of a grain (the defect volumes from Ref. [32] are summarized in Table 3.1). Therefore, bulk diffusion under a stress gradient enables plastic deformation (creep) that acts to relieve an applied stress.

The Nabarro-Herring creep rate, $\dot{\varepsilon}_{NH,\,x}$, due to a given defect, x, is expressed as:

$$\dot{\varepsilon}_{NH,\,x} = \frac{42|\Omega_x|D_x[x]}{k_B T d^2}\sigma \tag{3.1}$$

where σ is the applied stress, and d is the grain size. $[x]$ and Ω_x are the defect concentration (calculated in Section 3.1) and volume, respectively. D_x is the diffusivity of the defect. Due to the anisotropic nature of the U_3Si_2 system, D_x must be selected carefully. For Nabarro-Herring creep, diffusion of point defects must occur from one side of the grain to a perpendicular (not opposite) side. This requires the defect to traverse both the aa and cc crystallographic directions. Diffusion in a single direction would not results in creep. Therefore, the slowest mobility direction will be limiting. As such, the defect diffusivities used for creep are different to those used to assess the defect concentrations during cluster dynamics simulations, and are

Table 3.1: Parameters describing defect diffusivities in the creep model. Migration barriers, H_{mig}, attempt frequencies, v_{mig}, dimensionality, ξ, jump distance, α, number of jump sites, Z, and the defect volumes, Ω_x, are reported.

Defect	H_{mig} (eV)	v_{mig} (Hz)	α (Å)	ξ	Z	Ω_x (Å^3)
U_i	2.56	1.00×10^{14}	3.90	1	2	0.07
V_U	1.71	8.18×10^{12}	5.18	2	4	4.21
Si_i	2.91	1.00×10^{13}	3.90	1	8	4.09
V_{Si}	2.44	1.00×10^{13}	4.19	1	2	7.81

given in Table 3.1.

Separate contributions from different defects to Nabarro-Herring creep were assessed using Eq. (3.1) with the defect concentrations from Section 3.1, and are given by the following expressions:

$$\dot{\varepsilon}_{NH,\,V_U} = \frac{\sigma}{d^2} \cdot \left(1.055 \times 10^{-14} \cdot \exp\left(\frac{-2.774 \text{ eV}}{k_B T} \right) + 1.292 \times 10^{-53} \dot{F} \cdot \exp\left(\frac{-0.00467 \text{ eV}}{k_B T} \right) \right) \tag{3.2}$$

$$\dot{\varepsilon}_{NH,\,U_i} = \frac{\sigma}{d^2} \cdot 1.458 \times 10^{-17} \cdot \exp\left(\frac{-3.264 \text{ eV}}{k_B T} \right) \tag{3.3}$$

$$\dot{\varepsilon}_{NH,\,V_{Si}} = \frac{\sigma}{d^2} \cdot \left(4.733 \times 10^{-12} \cdot \exp\left(\frac{-4.104 \text{ eV}}{k_B T} \right) + 5.164 \times 10^{-55} \dot{F} \cdot \exp\left(\frac{-0.0547 \text{ eV}}{k_B T} \right) \right) \tag{3.4}$$

$$\dot{\varepsilon}_{NH,\,Si_i} = \frac{\sigma}{d^2} \cdot 5.329 \times 10^{-14} \cdot \exp\left(\frac{-3.294 \text{ eV}}{k_B T} \right) \tag{3.5}$$

where σ is the stress in Pa, T is the temperature in K, d is the grain size in m, $\dot{F}$ is the fission rate density in $\text{m}^{-3}\text{s}^{-1}$. Note that the irradiation enhanced contributions are nearly athermal. However, for numerical accuracy at low T, the non-zero activation energy must be included.

Figure 3.3 shows the creep rate due to various defects assuming $\dot{F} = 10^{19}$ $\text{m}^{-3}\text{s}^{-1}$ and $\sigma =$ 50 MPa. Given that the crystallographic direction with lower diffusivity is used for creep, the interstitial contributions are greatly lowered with respect to that of the vacancies (as compared to their relative self-diffusivities, Fig. 3.2, which used the highest diffusivity direction). Note that only vacancy contributions have an irradiation enhanced contribution, in line with the concentrations shown in Fig. 3.1. For both Si and U the dominant mechanism at low temperatures is irradiation enhanced vacancies. However, the irradiation enhanced contribution is so low that it will result in negligible creep. At high temperatures, U vacancies and Si interstitials dominate.

The total Nabarro-Herring creep rate for a given species is given by the sum of the interstitial and vacancy contributions. However, for stoichiometric redistribution of material both U and Si must diffuse. Therefore, the rate limiting factor for all temperatures studied is Si creep and the total Nabarro-Herring creep rate in U_3Si_2 is given by:

$$\dot{\varepsilon}_{NH} = \dot{\varepsilon}_{NH,\,V_{Si}} + \dot{\varepsilon}_{NH,\,Si_i} \tag{3.6}$$

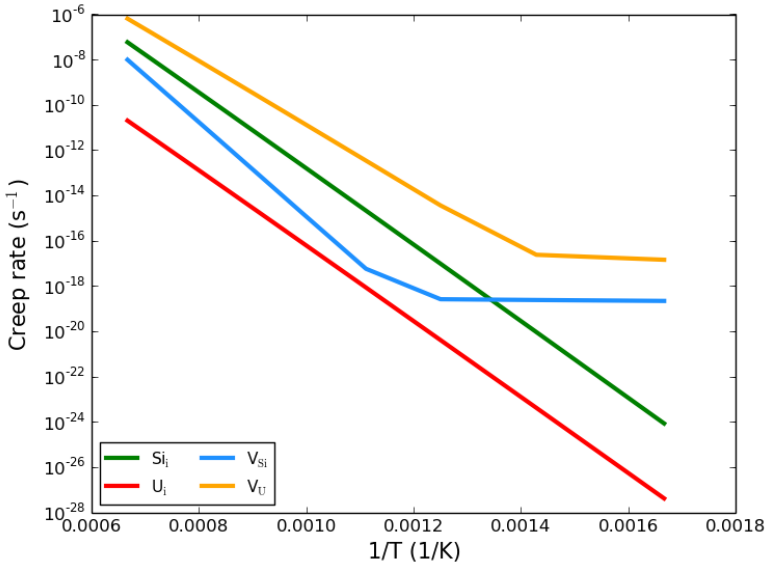

Figure 3.3: The Nabarro-Herring creep rate due to various point defects in U_3Si_2. Fit to the data are given by Equations (3.2) to (3.5).

The other contribution to diffusional creep is due to grain boundary diffusion (Coble creep). In previous work [33], MD simulations were carried out to predict the grain boundary diffusivity. The contribution to Coble creep for a given defect, x, is then given by:

$$\dot{\varepsilon}_{Coble,\,x} = \frac{42|\Omega_x| D_{GB} \pi \delta}{k_B T d^3} \sigma \tag{3.7}$$

where D_{GB} was fitted to the data in Ref. [33], δ is the grain boundary thickness (assumed to 1 nm). Other parameters have the same definition as in Eq. (3.1). The only difference between the various defects is due to the defect volume (as reported in Table 3.1). The resulting Coble creep rates for each defect are as follows:

$$\dot{\varepsilon}_{Coble,\,V_U} = \frac{\sigma}{d^3} \cdot 2.529 \times 10^{-24} \cdot \exp\left(\frac{-1.393 \text{ eV}}{k_B T}\right) \tag{3.8}$$

$$\dot{\varepsilon}_{Coble,\,U_i} = \frac{\sigma}{d^3} \cdot 4.204 \times 10^{-26} \cdot \exp\left(\frac{-1.393 \text{ eV}}{k_B T}\right) \tag{3.9}$$

$$\dot{\varepsilon}_{Coble,\,V_{Si}} = \frac{\sigma}{d^3} \cdot 4.691 \times 10^{-24} \cdot \exp\left(\frac{-1.393 \text{ eV}}{k_B T}\right) \tag{3.10}$$

$$\dot{\varepsilon}_{Coble,\,Si_i} = \frac{\sigma}{d^3} \cdot 2.456 \times 10^{-24} \cdot \exp\left(\frac{-1.393 \text{ eV}}{k_B T}\right) \tag{3.11}$$

Unlike Nabarro-Herring creep, the same grain boundary diffusivity is used for all defects, therefore, the only distinguishing parameter is the defect volume. As before, the total creep rate for a given species is given by the sum of the vacancy and interstitial contributions. Coble creep

is, thus, rate limited by uranium defects due to their smaller combined defect volume compared silicon defects. Therefore, the total Coble creep rate is given as such:

$$\dot{\varepsilon}_{Coble} = \frac{\sigma}{d^3} \cdot 2.571 \times 10^{-24} \cdot \exp\left(\frac{-1.393 \text{ eV}}{k_B T}\right) \tag{3.12}$$

The total diffusional creep rate is given as:

$$\dot{\varepsilon} = \dot{\varepsilon}_{NH} + \dot{\varepsilon}_{Coble} \tag{3.13}$$

Figure 3.4 shows the variation of Nabarro-Herring and Coble creep rates as function of temperature, for a stress of 50 MPa, a grain size of 20 μm, and a fission rate density of 10^{19} $m^{-3}s^{-1}$. These parameters have been selected as typical of LWR conditions and the U_3Si_2 microstructure, however they are variables that, when implemented in BISON, can be coupled to a grain growth model or a solid-mechanics model. It can be seen that at low temperatures the irradiation enhanced Nabarro-Herring creep mechanism dominates. However, at these temperatures the strain rate is so low that it will not result in any meaningful creep. At high temperatures, where non-negligible creep is more likely, Coble creep dominates.

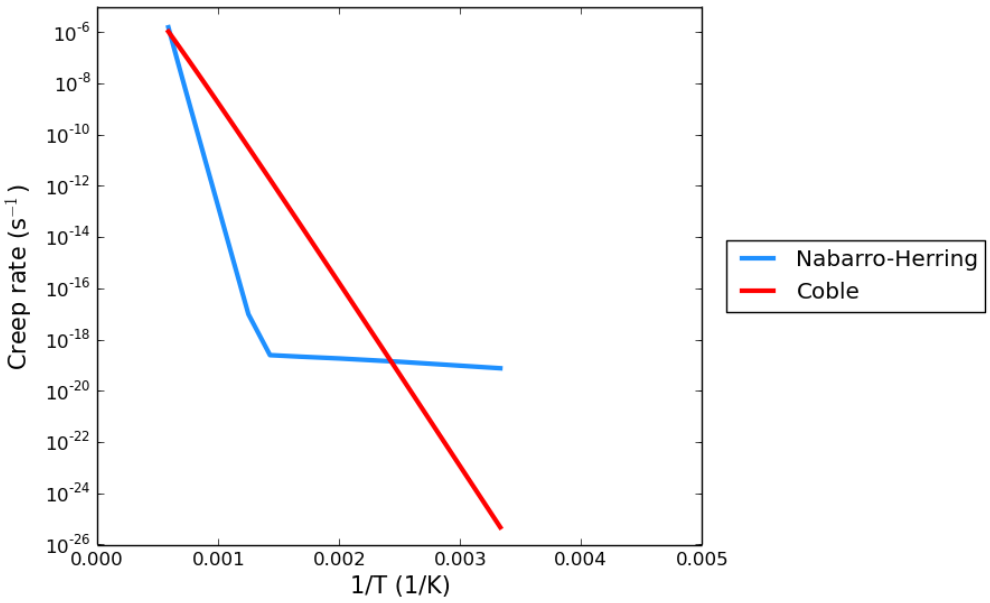

Figure 3.4: The Nabarro-Herring and Coble creep rates predicted for U_3Si_2.

3.3 Validation of creep model

To test the accuracy of our model, validation has been carried out against compression creep tests done at the University of South Carolina [1]. Table 3.2 shows the set of temperatures and stresses for the experiments. The values predicted by our model are also reported in Table 3.2,

Table 3.2: Validation of model against creep tests on U_3Si_2 [1]. Experimental temperatures (T), stresses (σ), and strain rates ($\dot{\varepsilon}_{Expt.}$) are provided in Ref. [1]. The strain rates from our model ($\dot{\varepsilon}_{Model}$) are also reported for the same conditions.

Creep test	σ (MPa)	T (K)	$\dot{\varepsilon}_{Expt.}$	$\dot{\varepsilon}_{Model}$
1	44.10	1218.37	8.7327×10^{-8}	2.6025×10^{-8}
2	71.77	1205.18	1.1134×10^{-7}	3.6761×10^{-8}
4	77.68	1122.24	1.9769×10^{-8}	1.5139×10^{-8}
5	57.69	1210.10	5.2848×10^{-8}	3.1163×10^{-8}
6	46.81	1173.58	1.9071×10^{-8}	1.6862×10^{-8}
7	45.65	1223.59	4.6836×10^{-8}	2.8470×10^{-8}
9	49.43	1223.56	2.8543×10^{-8}	3.0818×10^{-8}
11	27.36	1223.70	1.1998×10^{-8}	1.7083×10^{-8}
12	26.40	1273.60	1.8869×10^{-8}	2.7358×10^{-8}
13	47.77	1273.61	2.9740×10^{-8}	4.9508×10^{-8}

assuming a grain size of 20 μm and a fission rate density of 10^{19} $m^{-3}s^{-1}$. All of our model predictions are within one order of magnitude of the experimental data, with an average error of $\pm 40\%$. Given the exponential nature of an Arrhenius relationship, this represents very good agreement.

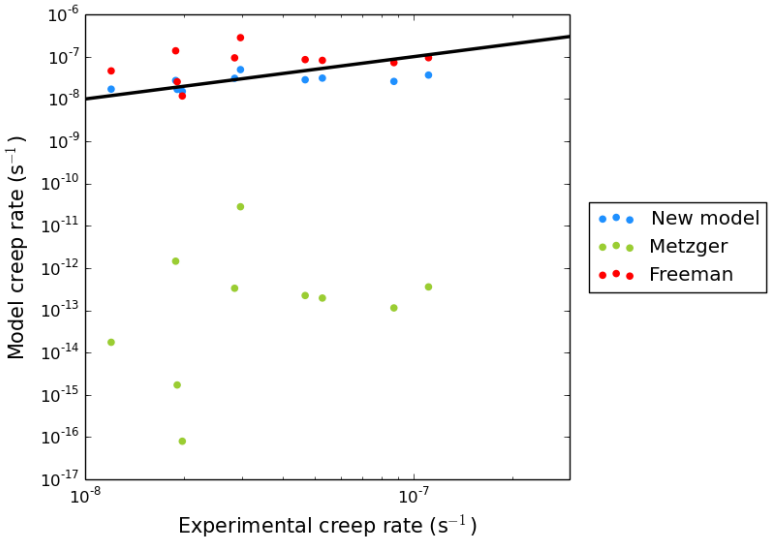

Figure 3.5: A parity plot comparing the modeled creep rate against the results from compressive creep tests [1]. The new model presented in this report is shown alongside the models from Freeman [2] and Metzger [3]. The solid line indicates perfect agreement between the experiment and the model.

Figure 3.5 is a parity plot comparing the model predictions (y-axis) with the experimental data (x-axis). The results using the new model presented in this report are shown in blue alongside

the previous models developed by Metzger [3] in green and Freeman [2] in red. The solid black line indicates perfect agreement between experiment and modeling. Compared to existing models, our model predicts slightly lower creep than the empirical correlation of Freeman et al. [2] and significantly more creep than the Metzger model [3]. A similar framework to the Metzger model [3] was used as the basis for our work but instead of using grain growth to estimate the diffusivities, it has been informed only by diffusivity data developed at the atomic scale. Figure 3.5 shows that application of the DFT and cluster dynamics data for point defect diffusivity improves the predictions of creep compared to experiment. Furthermore, the new model provides an improvement on the empirical Freeman model [2, 35] that was derived from a subset of the experimental data shown in Table 3.2. Additionally, the new model has the benefit of including the dependence of creep rate on grain size, which enables coupling to a grain growth model for U_3Si_2. Given the good agreement with experiment, the new model has been implemented in BISON for fuel performance simulations on U_3Si_2.

It should be noted that the creep model developed here does not account for creep due to dislocations, which could increase the predicted creep rate.

3.4 Implementation of creep model in BISON

The description of creep in U_3Si_2 given by Eq. (3.13) (informed by Eqs. (3.4) to (3.6) and (3.12)) was implemented into the BISON fuel performance to demonstrate the usage of the multiscale modeling approach from the atomistic scale through to the engineering scale. The newly developed model predicts similar creep rates when compared to separate effects creep tests (see Section 3.3). To illustrate the effect of U_3Si_2 creep under reactor operating conditions, two analyses of a 10 pellet rodlet are considered, one with no creep activated (i.e., the fuel is treated as elastic) and a second where the newly developed creep model is activated. The geometry of the rodlet is represented using a 2D-RZ axisymmetric assumption with a smeared fuel pellet column (i.e., dishes and chamfers are not explicitly modeled). Detailed specifications are included in Table 2.3, including the coolant and rod internal pressure conditions.

Due to the very high thermal conductivity of U_3Si_2 [36] the temperatures are low for typical LWR operating conditions (e.g., linear powers of 20-25 kW/m). Furthermore, the near-athermal term in Eq. (3.4) is very small. As such, for normal LWR linear powers virtually no creep is observed. Therefore, in this study, in order to increase the chance of observing creep the linear power supplied to the fuel is ramped up over 10,000 seconds from 0 to 35 kW/m and held for $\sim$3.2 years.

Figure 3.6 presents a) the predicted fuel outer diameter at the end of the simulation as well as b) the time history of the fuel centerline temperature during the simulation. One observes that the end-of-life diameter is slightly larger (< 0.01 mm) in the case with creep indicating that by computing creep there is an observable, but insignificant effect on the final fuel diameter. Similarly, the larger fuel diameter results in a lower average centerline temperature.

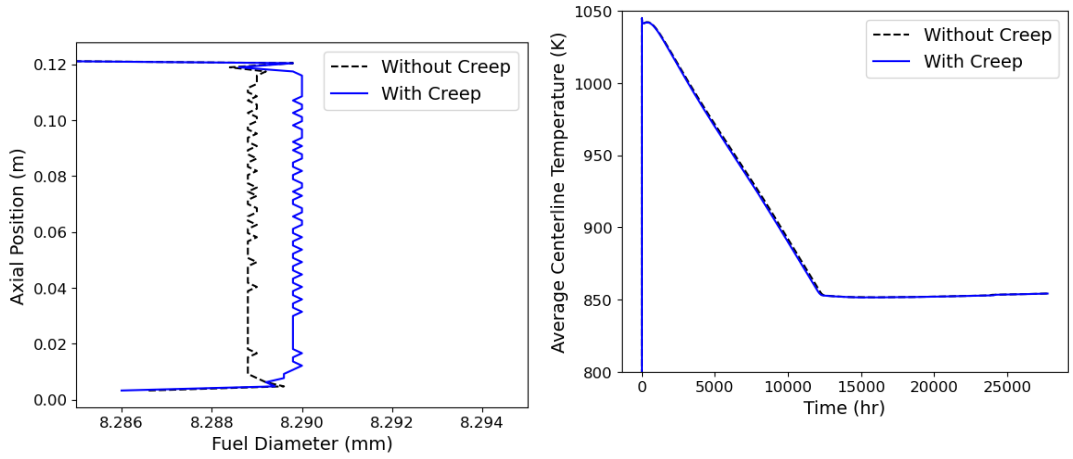

(a) (b)

Figure 3.6: The (a) end-of-life diameter of the fuel and (b) the time history of the average centerline temperature during BISON simulations.

4 Conclusions

U_3Si_2 is considered as an advanced nuclear fuel candidate due to its high thermal conductivity and high uranium density. These properties are beneficial for the performance and economics of nuclear fuel. However, due to the lack of experience of using U_3Si_2 as a nuclear fuel there is limited data for the thermophysical and thermomechanical properties that are required to build fuel performance modeling capability.

In this work, a multiscale approach has been used to develop a creep model based on atomic scale simulation data. A DFT-informed cluster dynamics model was used to predict the concentrations of defects under irradiation for in-reactor conditions. Based on the diffusivity of the irradiation-enhanced defect concentration in bulk U_3Si_2, a model for Nabarro-Herring creep was derived. Similarly, a Coble creep model was developed using MD simulation results for grain boundary diffusion from a previous milestone. The combined creep model captures the impact of fission rate, stress, and grain size on creep rate. It could, therefore, be coupled to a grain growth model enabling a more mechanistic understanding of creep in a reactor than is possible with the current empirical model. The new creep model compared very well with available experimental data. It has been implemented in BISON and tested for some simple power profiles, indicating that very limited creep will occur for LWR conditions.

Acknowledgments

Funding for this work was provided by the US Department of Energy, Office of Nuclear Energy NEAMS (Nuclear Energy Advanced Modeling and Simulation) program. Los Alamos National Laboratory, an affirmative action/equal opportunity employer, is operated by Triad National Security, LLC, for the National Nuclear Security Administration of the U.S. Department of Energy under Contract No. 89233218CNA000001.

References

[1] T. W. Knight, U_3Si_2 Fabrication and Testing for Implementation into the BISON Fuel Performance Code, Tech. rep. (2018). doi:doi:10.2172/1434631.

[2] R. A. Freeman, T. Martin, E. Roberts, T. W. Knight, Analysis of thermal creep for uranium silicide fuel using BISON, in: Proceedings of the International Congress on Advances in Nuclear Power Plants - ICAPP 2018, 2018.

[3] K. E. Metzger, Analysis Of Pellet Cladding Interaction And Creep Of U_3Si_2 Fuel For Use In Light Water Reactors, University of South Carolina Ph.D. thesis (2016).

[4] J. T. White, A. T. Nelson, J. T. Dunwoody, D. D. Byler, D. J. Safarik, K. J. Mcclellan, Thermophysical properties of U_3Si_2 to 1773 K, Journal of Nuclear Materials 464 (2015) 275–280.

[5] Y.-S. Kim, Uranium intermetallic fuels (U-Al, U-Si, U-Mo), in R Konings (Ed.), Comprehensive Nuclear Materials, 2012.

[6] J. Rest, A model for fission-gas-bubble behavior in amorphous uranium silicide compounds, Journal of Nuclear Materials 325 (2004) 107–117.

[7] T. C. Wiencek, R. F. Domagala, H. R. Thresh, Thermal Compatibility Studies of Unirradiated Uranium Silicide Dispersed in Aluminum, Nuclear Technology 71 (1985) 608–616.

[8] M. R. Finlay, G. L. Hofman, J. Rest, J. L. Snelgrove, Behaviour of Irradiated Uranium Silicide Fuel Revisited, in: International Meeting on Reduced Enrichment for Research and Test Reactors, 2002.

[9] J. Rest, G. L. Hofman, DART Model for Irradiation-Induced Swelling of Uranium Silicide Dispersion Fuel Elements, Nuclear Technology 126 (1999) 88–101.

[10] Y. S. Kim, G. L. Hofman, J. Rest, A. B. Robinson, Temperature and dose dependence of fission-gas-bubble swelling in U3Si2, Journal of Nuclear Materials 389 (2009) 443–449.

[11] G. L. Hofman, Crystal Structure stability and fission gas swelling in intermetallic uranium compounds, Journal of Nuclear Materials 140 (1986) 256–263.

[12] R. C. Birtcher, J. W. Richardson, M. H. Mueller, Amorphization of U_3Si_2 by ion or neutron irradiation, Journal of Nuclear Materials 230 (1996) 158–162.

[13] R. C. Birtcher, J. W. Richardson, M. H. Mueller, Amorphization of U_3Si by ion or neutron irradiation, Journal of Nuclear Materials 244 (1997) 251–257.

[14] M. R. Finlay, G. L. Hofman, J. L. Snelgrove, Irradiation behaviour of uranium silicide compounds, Journal of Nuclear Materials 325 (2004) 118–128.

[15] M. A. Feraday, G. H. Chalder, K. D. Cotnam, Irradiation Behavior of Cored U_3Si Fuel Elements, Nuclear Applications 4 (1968) 148–153.

[16] I. J. Hastings, J. R. MacEwan, L. R. Bourque, Effect of Swelling on Thermal Conductivity and Postirradiation Densification of U_3Si, Journal of the American Ceramic Society 55 (1972) 240–242.

[17] I. J. Hastings, Burnup and temperature dependence of swelling in U_3Si, Journal of Nuclear Materials 41 (1971) 195–202.

[18] R. B. Matthews, M. L. Swanson, Swelling of Uranium Silicide Fuel During Postirradiation Heating, Nuclear Technology 26 (1975) 278–286.

[19] E. S. Wood, J. T. White, C. J. Grote, A. T. Nelson, U_3Si_2 behavior in H_2O: Part I, flowing steam and the effect of hydrogen, Journal of Nuclear Materials 501 (2018) 404–412.

[20] A. T. Nelson, A. Migdisov, E. S. Wood, C. J. Grote, U_3Si_2 behavior in H_2O environments: Part II, pressurized water with controlled redox chemistry, Journal of Nuclear Materials 500 (2018) 81–91.

[21] C. Herring, Diffusional Viscosity of a Polycrystalline Solid, Journal of Applied Physics 21 (1950) 437-445.

[22] R. L. Coble, A Model for Boundary Diffusion Controlled Creep in Polycrystalline Materials, Journal of Applied Physics 34 (1963) 1679.

[23] D. Andersson, P. Garcia, X.-Y. Liu, G. Pastore, M. Tonks, P. Millett, B. Dorado, D. Gaston, D. Andrs, R. Williamson, R. Martineau, B. Uberuaga, C. Stanek, Atomistic modeling of intrinsic and radiation-enhanced fission gas (Xe) diffusion in $UO_{2\pm x}$: Implications for nuclear fuel performance modeling, Journal of Nuclear Materials 451 (2014) 225–242.

[24] M. Tonks, D. Andersson, R. Devanathan, R. Dubourg, A. El-Azab, M. Freyss, F. Iglesias, K. Kulacsy, G. Pastore, S. R. Phillpot, M. Welland, Unit mechanisms of fission gas release: Current understanding and future needs, Journal of Nuclear Materials 504 (2018) 300–317.

[25] R. Perriot, C. Matthews, M. W. D. Cooper, B. P. Uberuaga, C. R. Stanek, D. A. Andersson, Atomistic modeling of out-of-pile xenon diffusion by vacancy clusters in UO_2, Journal of Nuclear Materials 520 (2019) 96–109.

[26] C. Matthews, R. Perriot, M. W. D. Cooper, C. R. Stanek, D. A. Andersson, Cluster dynamics simulation of uranium self-diffusion during irradiation in UO_2, Journal of Nuclear Materials 527 (2019) 151787.

[27] C. Matthews, R. Perriot, M. Cooper, C. R. Stanek, D. A. Andersson, Cluster Dynamics Simulation of Xenon Diffusion During Irradiation in UO2, Journal of Nuclear Materials, Under Review.

[28] M. W. D. Cooper, C. Matthews, C. R. Stanek, D. A. Andersson, Modeling the plasticity and thermal creep of doped oxide nuclear fuel. CASL, Tech. rep. L3:FMC.FUEL.P19.04 (2019).

[29] M. W. D. Cooper, C. R. Stanek, J. A. Turnbull, B. P. Uberuaga, D. A. Andersson, Simulation of radiation driven fi ssion gas diffusion in UO 2 , ThO 2 and PuO_2, Journal of Nuclear Materials 481 (2016) 125–133.

[30] J. L. Wormald, A. I. Hawari, Examination of the impact of electron-phonon coupling on fission enhanced diffusion in uranium dioxide using classical molecular dynamics, Journal of Materials Research 30 (2015) 1485–1494.

[31] G. Martin, S. Maillard, L. V. Brutzel, P. Garcia, B. Dorado, C. Valot, A molecular dynamics study of radiation induced diffusion in uranium dioxide, Journal of Nuclear Materials 385 (2009) 351–357.

[32] D. A. Andersson, X. Liu, B. Beeler, S. C. Middleburgh, A. Claisse, C. R. Stanek, Density functional theory calculations of self- and Xe diffusion in U_3Si_2, Journal of Nuclear Materials 515 (2019) 312–325.

[33] M. W. D. Cooper, C. Matthews, C. R. Stanek, K. Gamble, B. Beeler, G. Pastore, Fission gas and creep in uranium silicide fuel, CASL Report L3:FMC.FUEL.P19.05, Tech. rep. (2019).

[34] H. Shimizu, The properties and irradiation behavior of U_3Si_2, Tech. rep. NAA-SR-10621 Atomics International (1965).

[35] K. A. Gamble, G. Pastore, M. W. D. Cooper, D. A. Andersson, CASL Milestone: AFT material model development and validation for priority fuel concepts, Tech. rep. L3:FMC.FUEL.P19.06 (2019).

[36] J. T. White, A. W. Travis, J. T. Dunwoody, A. T. Nelson, Fabrication and thermophysical property characterization of UN/U_3Si_2 composite fuel forms, Journal of Nuclear Materials 495 (2017) 463–474.